

# Multi-scale frequency separation network for image deblurring

Yanni Zhang<sup>1,\*</sup>, Qiang Li<sup>1,\*</sup>, Miao Qi<sup>1</sup>, Di Liu<sup>1</sup>, Jun Kong<sup>1,2,†</sup> and Jianzhong Wang<sup>1,†</sup>

<sup>1</sup>College of Information Science and Technology, Northeast Normal University, China

<sup>2</sup>Key Laboratory of Applied Statistics of MOE, Northeast Normal University, China

## Abstract

Image deblurring aims to restore the detailed texture information or structures from the blurry images, which has become an indispensable step in many computer-vision tasks. Although various methods have been proposed to deal with the image deblurring problem, most of them treated the blurry image as a whole and neglected the characteristics of different image frequencies. In this paper, we present a new method called multi-scale frequency separation network (MSFS-Net) for image deblurring. MSFS-Net introduces the frequency separation module (FSM) into an encoder-decoder network architecture to capture the low- and high-frequency information of image at multiple scales. Then, a simple cycle-consistency strategy and a sophisticated contrastive learning module (CLM) are respectively designed to retain the low-frequency information and recover the high-frequency information during deblurring. At last, the features of different scales are fused by a cross-scale feature fusion module (CSFFM). Extensive experiments on benchmark datasets show that the proposed network achieves state-of-the-art performance.

## 1. Introduction

The blur artifact caused by motion of camera/object or out-of-focus lens will affect the image quality and severely degrade the performance of downstream computer vision tasks, such as video surveillance, object detection and face recognition. Therefore, accurate and efficient image deblurring techniques which could restore the sharp images from their blurry counterparts have attracted much attention in both academic and industrial communities.

In the early studies, most image deblurring methods focused on estimating the blurry kernel by introducing some prior information [3, 15, 42, 48]. However, since the blur in an image may be induced by multiple reasons, image deblurring becomes a highly ill-posed problem and it is difficult to model the complex blur kernel by simple and linear

assumptions.

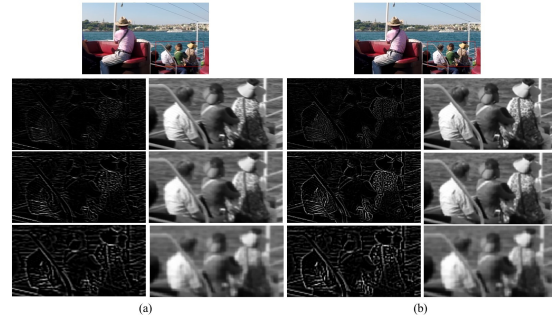


Figure 1. Detailed information of images from GoPro dataset with different frequencies and scales. (a) blurry image, (b) sharp image. From top to down are the original image, the high and low-frequency components of an image patch (marked as red box) with original, 1/2 and 1/4 scales, respectively. In this figure, the low-frequency component of each image is obtained by a linear low-pass Gaussian filter and the high-frequency component is obtained by subtracting the low-frequency component from the original image.

With the continuous development of deep learning, some deep convolutional neural networks (CNNs) [3, 10, 15, 22, 42, 48] have been adopted as blur kernel estimator and showed satisfied deblurring performance. However, these methods always need two stages to accomplish the image deblurring task. That is, they first interpolated the blur kernel using CNN and then utilized the estimated kernel for blurry image deconvolution. Therefore, the above methods may suffer from both high computational burden and inaccurate blur kernel estimation. More recently, some other CNN based image deblurring methods were proposed to directly learn the relationship between blurry and sharp images by an image-to-image regression manner [1, 2, 4, 8, 29, 31, 32, 49, 62]. Compared with other works, the advantage of image-to-image regression methods is that they could avoid the deblurring errors induced by inadequate blur kernel estimation. Besides, the CNN has also been combined with some other techniques for image deblurring. In [49, 56, 57], Recurrent Neural Network (RNN) was considered as a deconvolution operation to model the

\*Equal contribution authors. †Corresponding authors.

spatially variant blur. Inspired by Generative Adversarial Network (GAN), researchers in [16,27,41,49,50] employed the generative and discriminative models into the image deblurring framework, which could make the deblurred images more realistic and effectively improve the deblurring quality.

Although the aforementioned CNN based deblurring methods adopted various techniques to remove the blur from images, they all utilized the multi-scale strategy to capture image features in a coarse-to-fine way. In other words, they processed the image features of different sizes to progressively recover the texture and structures of the blurry image. The coarse-to-fine scheme is reasonable for image deblurring because it could treat different image features in different scales. The coarse features can be captured by image of reduced resolution, while the fine features are more suitable to be recovered in high resolution image. However, the differences of image information not only exist in the resolution scale aspect but also can be reflected by different frequencies. That is, the smoothly changing structure and outline of an image are mainly described by its low-frequency component, while the rapidly changing fine details of the image are usually described by its high-frequency component. Therefore, since the existing CNN based image deblurring methods dealt the image feature at each scale as a whole and neglected to distinguish image frequencies, their performance may not be optimal.

To overcome the above limitation, we propose a multi-scale frequency separation network (MSFS-Net) for image deblurring. MSFS-Net combines the multi-scale strategy with the frequency separation module (FSM) to capture different image features from both resolution scale and frequency aspects. Furthermore, different frequency information of the image is processed differently in our work. Specifically, a simple cycle consistent criterion is employed to maintain the low-frequency feature and a contrastive learning based module is proposed to progressively restore the high-frequency feature at different scales. Finally, a cross-scale feature fusion module (CSFFM) is also designed to better fuse the feature of different scales. Experimental results and ablation analysis on three benchmark datasets demonstrate that with the help of frequency separation module and other components in our method, the proposed MSFS-Net can achieve state-of-the-art performance.

Our main contributions are fourfold:

- We propose a frequency separation module (FSM) to divide the image features into low- and high-frequency components. Through embedding FSM into an encoder-decoder network architecture, our MSFS-Net can comprehensively capture image features of different frequencies and scales.
- To differentially deal with the various features, a cycle-consistency strategy and a contrastive learning mod-

ule (CLM) are proposed to constrain the low- and high-frequency features, respectively.

- Unlike some other methods which simply concatenate the image features of the same scale [10, 15, 22], we propose a cross-scale feature fusion module (CSFFM) to fuse the features of encoder and decoder from different scales, so that the multi-scale information can be better used to facilitate the deblurring.

- Extensive experiments are conducted to demonstrate the effectiveness of our proposed MSFS-Net and the modules in it.

## 2. Related work

### 2.1. Image Deblurring

Nowadays, the deep CNN models with image-to-image regression strategy have been proved to be effective for image deblurring task. The pioneer work was multi-scale CNN (MSCNN) proposed by Nah et al. [32]. MSCNN adopted a network architecture with three sub-networks to restore the sharp image in a coarse-to-fine manner, in which different sub-networks process images of different sizes. Inspired by MSCNN, Gao et al. [13] proposed a coarse-to-fine image deblurring network with selective parameter sharing and nested skip connections between different sub-networks. Instead of stacking multiple sub-networks, Kuldeep et al. [37] adopted an encoder-decoder backbone with dense deformable module (DDM) and self-attention (SA) module to improve the deblurring performance without significantly increasing the computational cost. Cho et al. [8] presented a multi-input multi-output U-net (MIMO-UNet) which utilizes a single U-Net (i.e., encoder-decoder with short connections) but multiple input and output images to handle the coarse-to-fine image deblurring. Chi et al. [7] utilized an encoder-decoder network to extract multi-scale image features, and then integrated the auxiliary and meta learning to enhance the deblurring performance. Chen et al. [4] also applied encoder-decoder architecture to implement multi-scale and multi-stage image restoration tasks by introducing a new normalization method. In order to achieve better deblurring effect, RNN is also introduced for deblurring task [23, 49, 57, 61]. Zhang et al. [57] proposed an image deblurring approach by combining CNN with RNN, in which four RNN layers are utilized to receive different directional sequence of CNN features. Tao et al. [49] proposed a scale-recurrent network (SRN) by introducing the long-short term memory (LSTM) and Res-Block into an encoder-decoder based deblurring model. The success of GAN also promoted image deblurring research. Kupyn et al. proposed a DeblurGAN [27] to model different blur sources, in which a CNN with encoder-decoder architecture is employed as generator and a convolutional patch-based classifier is adopted as discriminator. Based

on DeblurGAN, Deblurgan-v2 [28] was proposed to incorporate a double-scale discriminator and a feature pyramid network into GAN to achieve better deblurring result. In order to achieve a more effective deblurring, Shao et al. [43] also proposed a DeblurGAN+ which employed an opposite channel based discriminative prior and a more robust encoder-decoder network architecture.

## 2.2. Frequency Separation

An image can be decomposed into different frequency bands, and different frequency bands contain structures and textures with distinct complexities. Therefore, analyzing the image feature in frequency domain is a commonly used technique in many conventional low-level computer vision tasks. Recently, researchers have also proposed some deep learning based deblurring methods which consider the characteristics of different image frequency. [3, 42] employed CNN for blur kernel estimation in frequency domain and achieve satisfactory results. In image-to-image regression framework, Liu et al. [31] designed a two-stage method which first separates the high-frequency residual information from the blurry image and then adopt an encoder-decoder network to realize the high frequency information refinement. Zou et al. [62] utilized discrete wavelet transform to divide the dilated convolution features into four frequency bands, so that different frequency features can be refined independently. Nevertheless, the above two methods only separate the image frequency in the first or last layer of the network. Thus, they can only capture the image features of different frequencies from a specific scale and ignored the different image frequency features of multiple scales.

## 2.3. Contrastive Learning

Contrastive learning [20] is a widely used self-supervised strategy and has become an effective tool to handle some real-world problems. Motivated by the success of its application in representation learning [9, 14, 33, 59], some researchers have adopted contrastive learning to model the comparative relationships between features for computer vision tasks [5, 17, 18, 21]. Recently, Park et al. adopted contrastive learning in an image-to-image translation network [36]. Wu et al. [52] designed a network using contrastive learning to remove the haze from hazy image. Wang et al. [51] also applied contrastive learning to obtain invariant degradation representation in image super-resolution problem. Although these methods demonstrated that contrastive learning can help to improve the performance of some low-level vision tasks, there are few works employ contrastive learning in image deblurring problem. Therefore, how to make good use of contrastive learning to facilitate the performance of image deblurring is still needed to be studied.

# 3. Method

## 3.1. Motivation

In multi-scale and hierarchical image deblurring methods, researchers have realized that the images of different scales or spatial resolutions reflect diverse features [8, 13, 31, 32, 49, 57]. That is, the image with large scale and high spatial resolution contains fine feature while the image with small scale and low spatial resolution captures the coarse feature. Nevertheless, previous deblurring works seldom took the frequency information of image into consideration. In this study, we observe that the difference between blurry and sharp images lies in both the scale and frequency aspects. Take the images in Fig. 1 as an example, it can be seen that the low and high-frequency parts of an image at various scales exhibit very different features. In other words, the image with original size contains more detailed texture than the images with smaller sizes. Moreover, we can also find that the discrepancy between blurry and sharp images at the same scale is mainly reflected by their high-frequency components. Specifically, the high-frequency component of a sharp image always captures more clear texture and structures than the high-frequency component of a blurry image at the same scale, while the low-frequency components of the sharp and blurry images at the same scale are very similar. This phenomenon may due to that blurring can be regarded as a process of diffusing the information encoded in sharp edges across an image, which would not dramatically alter the smoothly changing structure and outline of the image [25]. To further justify our observation, we compare the entropy obtained by all samples with different frequencies and scales in GoPro dataset [32]. From the distributions in Fig. 2, we can find the similar observations with those in Fig. 1. That is, the Jensen–Shannon divergences between entropy distributions obtained by high-frequency components of sharp and blurry images are much larger than those obtained by low-frequency components of sharp and blurry images. Moreover, we can also see that the difference between entropy distributions of sharp and blurry images with large scale is greater than that with small image scale.

## 3.2. Overview

Motivated by the observation in Section 3.1, we propose a multi-scale frequency separation network (MSFS-Net), which makes full use of different frequency features at different image scales, to achieve better deblurring performance. Figure 3 shows the overall architecture of the MSFS-Net.

As can be seen from Fig. 3, the architecture of MSFS-Net is based on an encoder-decoder structure to hierarchically extract multi-scale image features. Firstly, a blurry image is input and a  $3 \times 3$  convolution is applied to get shallow

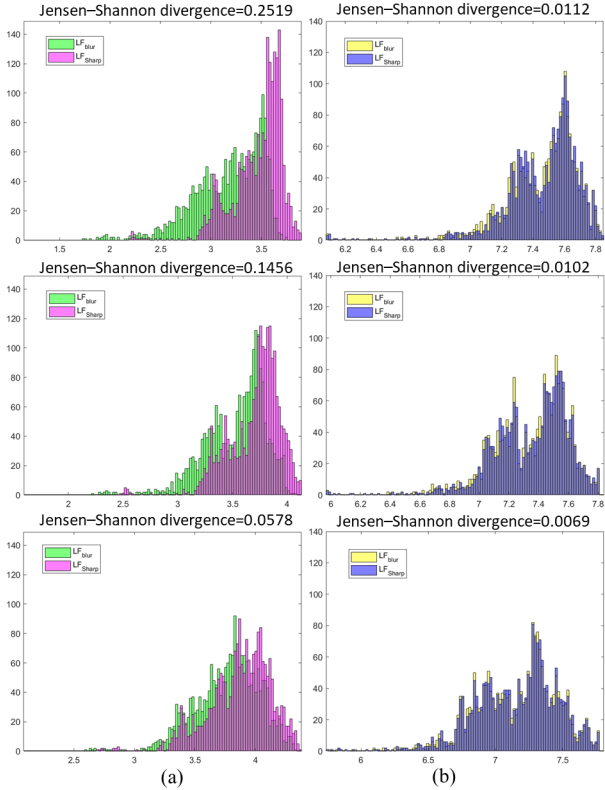


Figure 2. The distributions of entropy obtained by training samples in GoPro dataset. (a) From top to down are the distributions of entropy obtained by high-frequency components of sharp ( $HF_{sharp}$ ) and blurry ( $HF_{blur}$ ) images at original, 1/2 and 1/4 scales. (b) From top to down are the distributions of entropy obtained by low-frequency components of sharp ( $LF_{sharp}$ ) and blurry ( $LF_{blur}$ ) images at original, 1/2 and 1/4 scales.

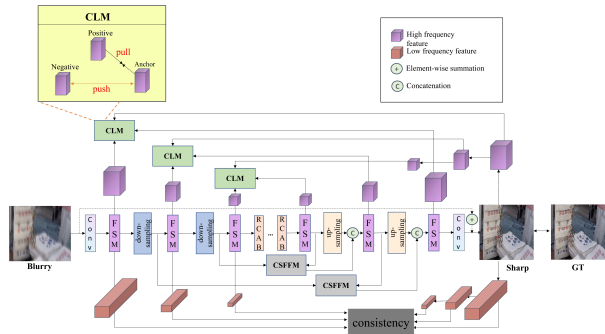


Figure 3. The architecture of the proposed MSFS-Net.

features. Then, the down-sampling module and frequency separation module (FSM) are combined in the encoder stage to progressively extract the low and high-frequency features of image at different scales. The down-sampling module consists of  $3 \times 3$  convolution with step 2 and LeakyRelu, and FSM is proposed to decompose the down-sampled features into different frequency (we will describe the details

of FSM in Section 3.3). After the encoder stage, we can get the latent feature of the input blurry image. In order to refine the latent feature, multiple RCABs [60] are further adopted to process the feature and improve the model capacity. Next, we use up-sampling module to achieve scale restoration of features in the decoder stage. The up-sampling module consists of RCAB with pixel-shuffle [45] and FSM is also adopted to decompose the restored features at each scale. Since the decoder stage requires delicately use of fine-grained details to reconstruct features, the cross-scale feature fusion module (CSFFM) is applied to connect features at different scales of encoder and decoder stages so that different context information can be passed to each other and well preserved. In order to minimize the loss of information and make the network converge rapidly, we fuse the raw image with the features after the last  $3 \times 3$  convolution of decoder by an element-wise summation. Last but most important, in order to take full advantage of low and high-frequency information, we reuse the encoder of network to obtain different frequency features of output sharp image at different scales, and two distinct strategies are carried out to constrain the low and high-frequency features in the intermedia layers of our network. On the one hand, since low-frequency features of the blurry and sharp images at the same scale are similar, a simple cycle-consistency criterion is utilized to ensure that the low-frequency features of the output sharp and input blurry images are not far away from each other. On the other hand, we propose a contrastive learning module (CLM) to regularize the high frequency features in the decoder stage. In CLM, we regard the high frequency features of encoder, decoder and generated sharp image at the same scale as negative, anchor and positive, respectively. Through the two opposite forces in CLM which pull the anchor closer to positive point and push the anchor farther away from negative point in the feature space, the interference of high frequency features in blurry image can be effectively removed. Here, it should be noted that we utilize the low and high-frequency components of output sharp image to constrain the intermedia features of different stages in the backbone network (i.e., low-frequency for encoder constraint and high-frequency for decoder constraint). This is because that the encoder is mainly used to extract context and outline information of the blurry image while the detailed information of sharp image is mostly generated by the decoder. Moreover, the cycle-consistency and CLM introduce multiple closed-loop structure in our network, which is helpful to reduce the solution space of our model [19].

### 3.3. Frequency Separation Module

The natural image can be divided into low and high-frequency components, and the output of a convolution layer can also be decomposed into features with different

spatial frequencies. Inspired by [6], Octave Convolution (OctConv) is used as the basic block of our frequency separation module (FSM). The structure of OctConv is shown in Fig. 4(a). Suppose  $X \in \mathbb{R}^{c_{in} \times h \times w}$  is the input feature in which  $h$  and  $w$  denote the spatial dimensions and  $c_{in}$  is the number of channels. OctConv first decomposes  $X$  into two parts, one is high-frequency  $X^H \in \mathbb{R}^{(1-\alpha_{in})c_{in} \times h \times w}$ , and the other part is low-frequency  $X^L \in \mathbb{R}^{\alpha_{in}c_{in} \times 0.5h \times 0.5w}$ . The parameter  $\alpha_{in}$  adjusts the number of channels in low and high-frequency. Then, the low and high-frequency features are processed by convolution and the information interaction between two frequencies will be carried out through pooling and up-sampling operations. The process of OctConv can be expressed by the following equations:

$$Y^H = f(X^H; W^{H \rightarrow H}) + up(f(X^L; W^{L \rightarrow H}), 2) \quad (1)$$

$$Y^L = f(X^L; W^{L \rightarrow L}) + f(pool(X^H, 2); W^{H \rightarrow L}) \quad (2)$$

where  $f(X;W)$  represents the convolution with kernel  $W$ , and the convolution kernel  $W$  is divided into  $W^H$  and  $W^L$  to convolve with  $X^H$  and  $X^L$  respectively.  $W^H$  can be further divided into  $W^{H \rightarrow H}$  and  $W^{L \rightarrow H}$  for intra- and inter-frequency processing. Similarly,  $W^L$  can also be divided into  $W^{L \rightarrow L}$  and  $W^{H \rightarrow L}$ . This process can realize the communication of low or high-frequency information. To deal with the mismatch between spatial scales of  $X^H$  and  $X^L$ ,  $pool(X,2)$  and  $up(X,2)$  are used.  $pool(X,2)$  represents average pooling with kernel size  $2 \times 2$  and stride 2, and  $up(X,2)$  is an up-sampling operation by a factor of 2. Through the above operations, the output high-frequency feature  $Y^H \in \mathbb{R}^{(1-\alpha_{out})c_{out} \times h \times w}$  and low-frequency feature  $Y^L \in \mathbb{R}^{\alpha_{out}c_{out} \times 0.5h \times 0.5w}$  can be obtained. The parameter  $\alpha_{out}$  also adjusts the output channel  $c_{out}$ .

Based on OctConv, the proposed FSM is shown in Fig. 4(b). First, a  $1 \times 1$  OctConv ( $\alpha_{in}=0, \alpha_{out}=0.5$ ) is utilized to divide the input feature into low and high-frequency parts. Then a  $3 \times 3$  OctConv ( $\alpha_{in}=0.5$  and  $\alpha_{out}=0.5$ ) is applied to accomplish the information exchange and updating. As a result, the low-frequency feature  $Y^L$  and high-frequency feature  $Y^H$  (shown in the yellow box in Fig. 4(b)) of the input feature can be obtained. Next, a  $1 \times 1$  OctConv ( $\alpha_{in}=0.5, \alpha_{out}=0$ ) is used to fuse the low and high frequency features into a whole for the subsequent down-sampling or up-sampling operation. At last, a residual connection is utilized to integrate the input feature with the output of the last OctConv, so that important information is not lost in FSM.

### 3.4. Cross-scale Feature Fusion Module

From the analysis and observation in previous sections, we know that the image features with different scales ex-

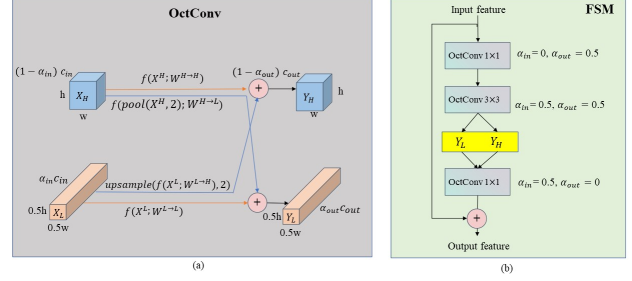


Figure 4. (a) The architecture of octave convolution (OctConv). (b) The architecture of frequency separation module (FSM).

hibit different characteristics. The image feature with large scale contains fine structures such as clear edges and textures. However, with the down-sampling of feature scale, the fine structures will gradually degenerate and only the coarse structures (such as the rough contours) in the image are left. Thus, the diversity between the blur and sharp images with large scale is much significant than small scale. In our study, different from other encoder-decoder based networks [13, 32, 57] which only fuse image features with the same scale in encoder and decoder stages, a cross-scale feature fusion module (CSFFM) is proposed to achieve the information fusion of features with different scales in different stages (encoder/decoder). The CSFFM is based on the idea of adaptive mix-up operation [55] and its specific process is shown in Fig. 5. The process is shown in the following equations:

$$f_{de-\frac{1}{2}} = up \left( \left[ \left( \begin{array}{c} sigmoid(\theta) * f_{en-\frac{1}{4}} + \\ (1 - sigmoid(\theta)) * f_{de-\frac{1}{4}} \end{array} \right), f_{en-\frac{1}{4}} \right] \right) \quad (3)$$

$$f_{de-1} = up \left( \left[ \left( \begin{array}{c} sigmoid(\gamma) * f_{en-\frac{1}{2}} + \\ (1 - sigmoid(\gamma)) * f_{de-\frac{1}{2}} \end{array} \right), f_{en-\frac{1}{2}} \right] \right) \quad (4)$$

where,  $f_{en-\frac{1}{i}}$  and  $f_{de-\frac{1}{i}}$  represent the features of  $1/i$  scale in encoder and decoder stages (the value of  $i$  is 1, 2 and 4 in our study),  $\theta$  and  $\gamma$  are the parameters optimizable by network,  $up$  represents the up-sampling operation and  $[\ ]$  denotes the concatenation. It can be seen from Fig. 5, Eq. 3 and Eq. 4 that CSFFM not only connect the features of encoder and decoder, but also realize the fusion of features at different scales. At the same time, in order to retain the important features of input image, we also concatenate the fused feature with the feature of encoder.

### 3.5. Contrastive Learning Module

The main idea of contrastive learning is to pull the positive paired samples together while push negative paired samples far apart in a feature space [52]. In our study, a

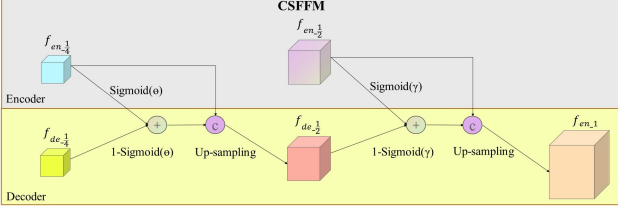


Figure 5. The architecture of the cross-scale feature fusion module.

contrastive learning module (CLM) is proposed to regularize the high-frequency features in decoder stage to get better restored images. According to Fig. 3, we can see that each CLM leverages three different high-frequency features at the same scale to construct the positive and negative pairs for contrast. Here, we take the high-frequency features obtained by the encoder stage, output sharp image and decoder stage as negative samples, positive samples, and anchors, respectively. The reasons for this design are two-fold. First of all, the high-frequency features in each scale of encoder stage are mainly captured from the blurry image, so the information contained in them are unclear and different from the sharp image. Secondly, since the output sharp image of backbone is closest to ground-truth, so the high-frequency features of it can be considered as guidance for the inter-media features in the decoder stage. Through the CLMs at multiple scales and the loss function associated with them, the adverse information in the high-frequency features of blurry image can be effectively suppressed.

### 3.6. Loss Functions

#### 3.6.1 Multi-scale Contrastive Loss for High-frequency Features

As mentioned in Section 3.5, we introduce the contrastive learning module (CLM) into our MSFS-Net for better image deblurring. Therefore, considering all CLMs at different scales, the multi-scale contrastive loss ( $\mathcal{L}_{high}$ ) for regularizing the high-frequency features in the network can be expressed by the following equation:

$$\mathcal{L}_{high} = \min \sum_{k=0}^2 \frac{\mathcal{L}_1(f_k^{anchor}, f_k^{positive})}{\mathcal{L}_1(f_k^{anchor}, f_k^{negative})} \quad (5)$$

where  $\times k$  represents the scale level of feature,  $f_k^{anchor}$  represents the high-frequency feature of  $\frac{1}{2^k}$  scale in the decoder stage,  $f_k^{positive}$  represents the high-frequency feature of  $\frac{1}{2^k}$  scale got by output sharp image,  $f_k^{negative}$  represents the high-frequency feature of  $\frac{1}{2^k}$  scale in the encoder stage,  $\mathcal{L}_1$  represents the  $\mathcal{L}_1$ -distance. In Eq.5, the numerator and denominator are utilized to pull the  $f_k^{anchor}$  and  $f_k^{positive}$  together and push the  $f_k^{anchor}$  and  $f_k^{negative}$  apart, respectively.

#### 3.6.2 Multi-scale Consistent Loss for Low-frequency Features

Since the low frequency features often reflect the outline and rough contour information of an image. The difference between the low-frequency features of blurry and sharp images is not obvious. Inspired by cycle-consistency, we minimize the  $\mathcal{L}_1$  distance between the low-frequency features in encoder stage and those generated by the output sharp image, so that the low-frequency features can be maintained during deblurring. Therefore, the multi-scale loss for low-frequency features can be expressed by:

$$\mathcal{L}_{low} = \min \sum_{k=0}^2 ||f_k^{en,low} - f_k^{low}||_1 \quad (6)$$

where  $k$  represents scale level,  $f_k^{en,low}$  represents the low-frequency feature of  $\frac{1}{2^k}$  scale in the encoder stage,  $f_k^{low}$  represents the low-frequency feature of  $\frac{1}{2^k}$  scale got by output sharp image. Furthermore, we should point out that since the input blurry image and output sharp image are both decomposed into multi-scale low and high-frequency components in our model, the consistent loss of low-frequency features in Eq. (6) will lead the diversity of blurry and sharp images to be mainly reflected by their high-frequency components at each scale, which could also facilitate our contrast learning module for high-frequency features.

#### 3.6.3 The Final Loss of MSFS-Net

At last, the total loss function used to train our MSFS-Net can be defined as:

$$\mathcal{L}_{total} = \lambda_1 \mathcal{L}_{high} + \lambda_2 \mathcal{L}_{low} + \min ||I - G||_1 \quad (7)$$

where  $\lambda_1 = \lambda_2$  are set as 0.005 by experiment,  $I$  represents the output of our network and  $G$  is the ground-truth, the  $\mathcal{L}_1$  is applied to minimize the loss between the recovered image and ground-truth.

### 3.7. Comparison with other methods

To highlight the novelty of the proposed model, we compare MSFS-Net with some related methods. First, though the frequency separation has been adopted in some works to deal with image restoration problem such as super-resolution [11, 30, 34, 39] and deraining [12], they only decomposed different frequency information from image features at a specific size. Thus, the characteristics of image features at different scales are neglected in them. Besides, for the methods which considered the frequency information of images in deblurring task [31, 62], they either only focused on high-frequency features or treated different frequency features of an image with the same strategy. Hence,

they are still different from our proposed method. Second, contrastive learning has also been employed in some image-to-image regression tasks [36, 52]. However, these methods merely leveraged the contrastive learning to regularize the final output rather than the intermedia layers of the network. Besides, the different frequencies of multi-scale image features are ignored in them. The last technique related to our work is the perceptual loss [26] which also utilizes a multi-layer network to extract the features of network’s output. Nevertheless, the differences between perceptual loss and our work are also apparent. The aim of perceptual loss is to measure the visual difference between the network’s output and the ground-truth by features extracted from a pre-trained deep neural network (i.e., VGG [46]). Hence, it cannot be adopted to constrain the features obtained by intermedia layers of backbone network. Furthermore, perceptual loss also overlooks the different frequency information of the image.

## 4. Experiments

### 4.1. Dataset and implementation details

We use the training set in GoPro [32] dataset to train our model and the test set to test the model. Besides, HIDE [44] and RealBlur [40] datasets are also employed to evaluate our model. GoPro dataset contains 3214 pairs of blurry and sharp images, in which the training set and test set consist of 2103 and 1111 pairs, respectively. HIDE dataset consists of 8422 pairs of blurry and sharp images and these images are carefully selected from 31 high-fps videos. RealBlur dataset consists of two subsets: RealBlur-J and RealBlur-R. For implementation details, the Adam optimizer with parameter setting as  $\beta_1=0.9$ ,  $\beta_2=0.9$ ,  $\epsilon=1e-8$  is used to optimize our network. The epochs and batch size are set as 3000 and 4 respectively. The initial learning rate is set as  $1e-4$  and decreased by the factor of 0.5 at every 500 epochs.

### 4.2. Quantitative and qualitative evaluation

#### 4.2.1 GoPro dataset

To demonstrate the effectiveness of the proposed MSFS-Net, we compare the performance of our method with some state-of-the-art algorithms on GoPro dataset. The quantitative comparison result is listed in Table 1, and some visual comparisons are shown in Fig. 6. In our experiment, the PSNR and SSIM results of all comparison methods are directly quoted from their original version in corresponding literatures.

From Table 1, we can see that the deblurring performance of our method is superior to other state-of-the-art methods. The advantage of MSFS-Net can be attributed to the following reasons. First, although some comparison methods [4, 7, 8, 13, 24, 35, 37, 38, 49, 53, 56] utilize the encoder-decoder network structure to extract multi-scale

features of the image for deblurring, they only adopt a simple skip connection mechanism to concatenate the features with the same scale in encoder and decoder. Nevertheless, thanks to the CSFFM in our model, the features of different stages (i.e., encoder and decoder) with different scales can be better fused. Therefore, the proposed MSFS-Net performs better than them. Second, the methods in [27, 28, 32, 47, 54, 57, 58] integrate the image features with different scales by some sophisticated network structure and modules. However, they treat the image as a whole and neglect the characteristics of different image frequencies. Thus, their performance is inferior to our model which makes full use of the low- and high-frequency information separated by FSM. Third, the method in [31] considers the frequency information in image deblurring problem. But it only focuses the high-frequency image features. Although SDWNet [62] utilizes the wavelet transformation for image frequency separation, it processes the low- and high-frequency image features using the same network. Hence, the deblurring results obtained by the above two methods are still not optimal. Besides, the methods in [62] and [31] only capture image frequency information at the first or last layer of the network and ignore the multi-scale frequency features of the image, which may also decrease their performance. At last, the proposed MSFS-Net can capture different frequency features of the image at multiple scales and designs different strategies (i.e., contrast learning and consistent loss) to handle them separately. Thus, it achieves the best deblurring result in Table 1.

Through the visual comparison in Fig. 6, we can see that our MSFS-Net outperforms other methods. For example, by comparing the deblurred images contain in the first and second lines of Fig. 6, it can be found that our model can restore more detailed structures in the face and clearer contours of the letters. Moreover, from the deblurred results in the third and fourth lines of Fig. 6, we can see that our model not only gets clearer contour of car and billboard, but also achieves better restoration for the image deformation and artifacts caused by severe object motion or camera shake.

In Fig. 7, we show the entropy distributions of low- and high-frequency components obtained by sharp images and deblurred images of our MSFS-Net. Through comparing the results with those in Fig. 2, we can see that our proposed method can effectively narrow the gap between the sharp and blurry images. That is, the Jensen-Shannon divergencies between entropy distributions of different frequencies at each scale are much smaller than those in Fig. 2.

#### 4.2.2 HIDE dataset

Following some other works [13, 27, 28, 32, 35, 40, 47, 49, 54, 56, 58, 62], we also evaluate our GoPro-trained MSFS-

Table 1. Performance comparison with state-of-the-art methods on GoPro dataset.

Methods	PSNR	SSIM
DeblurGAN [27]	28.70	0.927
Nah et al. [32]	29.08	0.914
Zhang et al. [57]	29.19	0.931
DeblurGAN-v2 [28]	29.55	0.934
Yuan et al. [53]	29.81	0.937
DMPHN [56]	30.21	0.935
SRN [49]	30.26	0.934
Liu et al. [31]	30.31	0.920
Gao et al. [13]	30.92	0.942
DBGAN [58]	31.10	0.942
MT-RNN [35]	31.15	0.945
SDWNet [62]	31.26	0.966
Kuldeep et al. [37]	31.76	0.953
Jiang et al. [24]	31.79	0.949
Suin et al. [47]	31.85	0.948
SPAIR [38]	32.06	0.953
Chi et al. [7]	32.50	0.958
MPRNet [54]	32.66	0.959
MIMO-UNet++ [8]	32.68	0.959
HINet [4]	32.71	0.959
<b>MSFS-Net</b>	<b>32.73</b>	<b>0.959</b>



Figure 6. Visual comparison of the deblurring results on GoPro dataset.

Net on HIDE dataset and compare its performance with other approaches. From the experimental results in Table 2 and visual comparisons in Fig. 8, we can clearly see the advantage of the proposed method. That is, our MSFS-Net can restore more detailed information from the blurry images and obtains better PSNR and SSIM results than other methods. According to the analysis in Section 4.2.1, this improvement is due to the multi-scale frequency separation, contrasting learning and cross-scale feature fusion modules proposed in our method.

Table 2. Performance comparison on HIDE dataset.

Methods	PSNR	SSIM
DeblurGAN [27]	24.51	0.871
Nah et al. [32]	25.73	0.874
DeblurGAN-v2 [28]	26.61	0.875
SRN [49]	28.36	0.915
Shen et al [40]	28.89	0.930
DBGAN [58]	28.94	0.915
SDWNet [62]	28.99	0.957
Gao et al. [13]	29.11	0.913
MT-RNN [35]	29.15	0.918
DMPHN [56]	29.09	0.924
Suin et al. [47]	29.98	0.930
Chi et al. [7]	30.55	0.935
MPRNet [54]	30.96	0.939
<b>MSFS-Net</b>	<b>31.05</b>	<b>0.941</b>

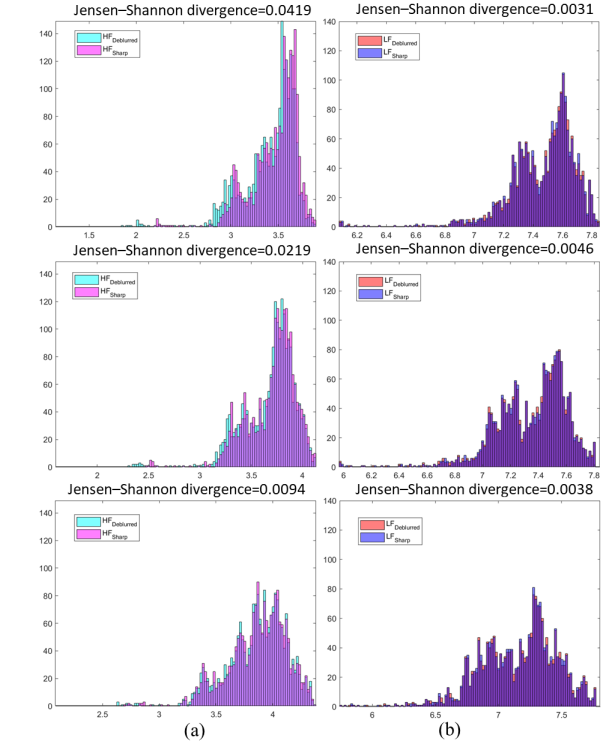


Figure 7. The distributions of entropy obtained by training samples in GoPro dataset. (a) From top to down are the distributions of entropy obtained by high-frequency components of sharp ( $HF_{sharp}^n$ ) and deblurred ( $HF_{Deblurred}^n$ ) images at original, 1/2 and 1/4 scales. (b) From top to down are the distributions of entropy obtained by low-frequency components of sharp ( $LF_{sharp}^n$ ) and deblurred ( $LF_{Deblurred}^n$ ) images at original, 1/2 and 1/4 scales.



Figure 8. Visual comparison of the deblurring results on HIDE dataset.

### 4.2.3 RealBlur dataset

In order to further test the generalization ability of the proposed MSFS-Net to real blurry images, we test the performance of our method on RealBlur dataset. The quantitative comparisons between MSFS-Net and other methods are shown in Table 3. Similar to Section 4.2.2, the networks in this experiment are all trained by GoPro dataset for a fair comparison. It can be found from Table 3 that our model achieves the best experimental results on both RealBlur-R and RealBlur-J subsets.



Table 3. Performance comparison on RealBlur dataset.

Methods	RealBlur-R		RealBlur-J	
	PSNR	SSIM	PSNR	SSIM
Nah et al. [32]	32.51	0.841	27.87	0.827
DeblurGAN [27]	33.79	0.903	27.97	0.834
DeblurGAN-v2 [28]	35.26	0.944	28.70	0.866
Zhang et al. [57]	35.48	0.947	27.80	0.847
SRN [49]	35.66	0.947	28.56	0.867
DMPHN [56]	35.70	0.948	28.42	0.860
MPRNet [54]	35.99	0.952	28.70	0.873
<b>MSFS-Net</b>	<b>36.02</b>	<b>0.959</b>	<b>28.97</b>	<b>0.908</b>

### 4.3. Ablation study and analysis

In this section, we conduct several experiments to evaluate the effectiveness of the components proposed in our MSFS-Net. First, we directly replace FSM with the traditional convolution operation in our network, which means we don't decompose the image into different frequency features, but just extract features from the whole image. As a result, the CLM and consistency constraints which are specifically designed for high- and low-frequency features are also neglected. Secondly, we remove CSFFM from the network to ignore the fusion of information from different scales and layers. Then, we abandon CLM in our model, which means we don't use the idea of contrast learning to supervise the high frequency features in the intermedia layers. Finally, the consistency constraint for low-frequency features is discarded.

Through the above settings, we can get four new network structures (MSFS-Net without FSM, without CSFFM, without CLM and without Consistency). In order to fairly compare their performance, we use the same parameter settings to train the four networks. The results of ablation experiment on GoPro dataset are shown in Table 4. From this table, we can find that FSM, CSFFM, CLM and Consistency are all essential to our MSFS-Net. Without FSM, the PSNR obtained by our model reduces by 2.93dB. This means separating the image into different frequency domains and utilizing different strategies to deal with them is crucial for deblurring problem. Besides, the removal of CSFFM also deteriorates the performance of our model. This is due to CSFFM can make connections between features at different stages and scales, which results in a better information fusion. Finally, we can see that the absence of Consistency constraint or CLM also has an adverse impact on the deblurring result of the proposed network. This justifies that constraining the low- and high-frequency features in the intermediate layers with contrastive learning and consistency criterion are both important for improving the deblurring performance.

## 5. Conclusion

In this work, we propose a multi-scale frequency separation network for image deblurring (MSFS-Net). In or-

Table 4. Comparison of different ablations of MSFS-Net on GoPro dataset.

	FSM	CSFFM	CLM	Consistency	PSNR	SSIM
×	✓	-	-	-	29.80	0.917
✓	×	✓	✓	✓	30.22	0.891
✓	✓	×	×	✓	31.08	0.911
✓	✓	✓	×	×	31.54	0.913
✓	✓	✓	✓	✓	<b>32.73</b>	<b>0.959</b>

der to make the network make full use of the low and high frequency information of features, we propose frequency separation module (FSM) to further separate features. At the same time, in order to make shallow features and deep features communicate with each other without losing information, cross-scale feature fusion module (CSFFM) is proposed to realize feature connection. In addition, the contrastive learning and cycle-consistency are designed based the method to learn the difference between low and high frequency information. The contrastive learning module (CLM) can achieve better supervision for high frequency features and cycle-consistency can implement the supervision for low frequency features. Experiments on three datasets show that MSFS-Net achieves good results in image deblurring task.

In the future, we will apply our MSFS-Net to other image restoration tasks (such as deraining, dehazing and denoising) to further test its generalization ability. Besides, how to incorporate some novel backbone networks (such as Vision Transformer) into our model to improve its feature extraction power is another interesting topic for our feature study.

## References

- [1] A. Abuolaim and M. S. Brown. Defocus deblurring using dual-pixel data. *Springer, Cham*, 2020. **1**
- [2] J. Cai, W. Zuo, and L. Zhang. Dark and bright channel prior embedded network for dynamic scene deblurring. *IEEE Transactions on Image Processing*, PP(99):1–1, 2020. **1**
- [3] Ayan Chakrabarti. A neural approach to blind motion deblurring. In *European conference on computer vision*, pages 221–235. Springer, 2016. **1, 3**
- [4] L. Chen, X. Lu, J. Zhang, X. Chu, and C. Chen. Hinet: Half instance normalization network for image restoration. 2021. **1, 2, 7, 8**
- [5] Ting Chen, Simon Kornblith, Mohammad Norouzi, and Geoffrey Hinton. A simple framework for contrastive learning of visual representations. In *International conference on machine learning*, pages 1597–1607. PMLR, 2020. **3**
- [6] Yunpeng Chen, Haoqi Fan, Bing Xu, Zhicheng Yan, Yanis Kalantidis, Marcus Rohrbach, Shuicheng Yan, and Jiashi Feng. Drop an octave: Reducing spatial redundancy in convolutional neural networks with octave convolution. In *Proceedings of the IEEE/CVF International Conference on Computer Vision*, pages 3435–3444, 2019. **5**
- [7] Zhixiang Chi, Yang Wang, Yuanhao Yu, and Jin Tang. Test-time fast adaptation for dynamic scene deblurring via meta-

- auxiliary learning. In *Proceedings of the IEEE/CVF Conference on Computer Vision and Pattern Recognition*, pages 9137–9146, 2021. 2, 7, 8
- [8] S. J. Cho, S. W. Ji, J. P. Hong, S. W. Jung, and S. J. Ko. Rethinking coarse-to-fine approach in single image deblurring. 2021. 1, 2, 3, 7, 8
- [9] Carl Doersch, Abhinav Gupta, and Alexei A Efros. Unsupervised visual representation learning by context prediction. In *Proceedings of the IEEE international conference on computer vision*, pages 1422–1430, 2015. 3
- [10] R. Fattal and A. Goldstein. Blur-kernel estimation from spectral irregularities, 2015. 1, 2
- [11] Manuel Fritsche, Shuhang Gu, and Radu Timofte. Frequency separation for real-world super-resolution. In *2019 IEEE/CVF International Conference on Computer Vision Workshop (ICCVW)*, pages 3599–3608. IEEE, 2019. 6
- [12] Xueyang Fu, Jiabin Huang, Xinghao Ding, Yinghao Liao, and John Paisley. Clearing the skies: A deep network architecture for single-image rain removal. *IEEE Transactions on Image Processing*, 26(6):2944–2956, 2017. 6
- [13] Hongyun Gao, Xin Tao, Xiaoyong Shen, and Jiaya Jia. Dynamic scene deblurring with parameter selective sharing and nested skip connections. In *Proceedings of the IEEE/CVF Conference on Computer Vision and Pattern Recognition*, pages 3848–3856, 2019. 2, 3, 5, 7, 8
- [14] Spyros Gidaris, Praveer Singh, and Nikos Komodakis. Unsupervised representation learning by predicting image rotations. *arXiv preprint arXiv:1803.07728*, 2018. 3
- [15] Dong Gong, Jie Yang, Lingqiao Liu, Yanning Zhang, Ian Reid, Chunhua Shen, Anton Van Den Hengel, and Qinfeng Shi. From motion blur to motion flow: A deep learning solution for removing heterogeneous motion blur. In *Proceedings of the IEEE conference on computer vision and pattern recognition*, pages 2319–2328, 2017. 1, 2
- [16] G. Gong and K. Zhang. Local blurred natural image restoration based on self-reference deblurring generative adversarial networks. In *2019 IEEE International Conference on Signal and Image Processing Applications (ICSIPA)*, 2019. 2
- [17] Jean-Bastien Grill, Florian Strub, Florent Althé, Corentin Tallec, Pierre Richemond, Elena Buchatskaya, Carl Doersch, Bernardo Avila Pires, Zhaohan Guo, Mohammad Gheshlaghi Azar, et al. Bootstrap your own latent—a new approach to self-supervised learning. *Advances in Neural Information Processing Systems*, 33:21271–21284, 2020. 3
- [18] J. B. Grill, F. Strub, F. Althé, C. Tallec, P. H. Richemond, E. Buchatskaya, C. Doersch, B. A. Pires, Z. D. Guo, and M. G. Azar. Bootstrap your own latent: A new approach to self-supervised learning. 2020. 3
- [19] Yong Guo, Jian Chen, Jingdong Wang, Qi Chen, Jiezhong Cao, Zeshuai Deng, Yanwu Xu, and Mingkui Tan. Closed-loop matters: Dual regression networks for single image super-resolution. In *Proceedings of the IEEE/CVF conference on computer vision and pattern recognition*, pages 5407–5416, 2020. 4
- [20] R. Hadsell, S. Chopra, and Y. Lecun. Dimensionality reduction by learning an invariant mapping. In *2006 IEEE Computer Society Conference on Computer Vision and Pattern Recognition (CVPR'06)*, 2006. 3
- [21] Olivier Henaff. Data-efficient image recognition with contrastive predictive coding. In *International Conference on Machine Learning*, pages 4182–4192. PMLR, 2020. 3
- [22] M Hradiš. Convolutional neural networks for direct text deblurring. In *British Machine Vision Conference*, 2015. 1, 2
- [23] Tae Hyun Kim, Kyoung Mu Lee, Bernhard Scholkopf, and Michael Hirsch. Online video deblurring via dynamic temporal blending network. In *Proceedings of the IEEE International Conference on Computer Vision*, pages 4038–4047, 2017. 2
- [24] Zhe Jiang, Yu Zhang, Dongqing Zou, Jimmy Ren, Jiancheng Lv, and Yebin Liu. Learning event-based motion deblurring. In *Proceedings of the IEEE/CVF Conference on Computer Vision and Pattern Recognition*, pages 3320–3329, 2020. 7, 8
- [25] B Jka, B JI, and B Sy. Single-image deblurring with neural networks: A comparative survey - sciencedirect. *Computer Vision and Image Understanding*, 2020. 3
- [26] J. Johnson, A. Alahi, and L. Fei-Fei. Perceptual losses for real-time style transfer and super-resolution. In *European Conference on Computer Vision*, 2016. 7
- [27] O. Kupyn, V. Budzan, M. Mykhailych, D. Mishkin, and J. Matas. Deblurgan: Blind motion deblurring using conditional adversarial networks. *IEEE*, 2018. 2, 7, 8, 9
- [28] O. Kupyn, T. Martyniuk, J. Wu, and Z. Wang. Deblurgan-v2: Deblurring (orders-of-magnitude) faster and better. *IEEE*, 2019. 3, 7, 8, 9
- [29] D. Li, C. Xu, K. Zhang, X. Yu, and H. Li. Arvo: Learning all-range volumetric correspondence for video deblurring. 2021. 1
- [30] Xin Li, Xin Jin, Tao Yu, Simeng Sun, Yingxue Pang, Zhizheng Zhang, and Zhibo Chen. Learning omnifrequency region-adaptive representations for real image super-resolution. In *AAAI Press*, volume 35, pages 1975–1983, 2021. 6
- [31] K. H. Liu, C. H. Yeh, J. W. Chung, and C. Y. Chang. A motion deblur method based on multi-scale high frequency residual image learning. *IEEE Access*, PP(99):1–1, 2020. 1, 3, 6, 7, 8
- [32] S. Nah, T. H. Kim, and K. M. Lee. Deep multi-scale convolutional neural network for dynamic scene deblurring. *IEEE Computer Society*, 2016. 1, 2, 3, 5, 7, 8, 9
- [33] Mehdi Noroozi, Hamed Pirsiavash, and Paolo Favaro. Representation learning by learning to count. In *Proceedings of the IEEE International Conference on Computer Vision*, pages 5898–5906, 2017. 3
- [34] Yingxue Pang, Xin Li, Xin Jin, Yaojun Wu, Jianzhao Liu, Sen Liu, and Zhibo Chen. Fan: frequency aggregation network for real image super-resolution. In *European Conference on Computer Vision*, pages 468–483. Springer, 2020. 6
- [35] D. Park, U. K. Dong, J. Kim, and S. Y. Chun. *Multi-Temporal Recurrent Neural Networks for Progressive Non-uniform Single Image Deblurring with Incremental Temporal Training*. *Computer Vision – ECCV 2020*, 2020. 7, 8

- [36] Taesung Park, Alexei A Efron, Richard Zhang, and Jun-Yan Zhu. Contrastive learning for unpaired image-to-image translation. In *European Conference on Computer Vision*, pages 319–345. Springer, 2020. 3, 7
- [37] Kuldeep Purohit and AN Rajagopalan. Region-adaptive dense network for efficient motion deblurring. In *Proceedings of the AAAI Conference on Artificial Intelligence*, volume 34, pages 11882–11889, 2020. 2, 7, 8
- [38] Kuldeep Purohit, Maitreya Suin, AN Rajagopalan, and Vishnu Naresh Boddeti. Spatially-adaptive image restoration using distortion-guided networks. In *Proceedings of the IEEE/CVF International Conference on Computer Vision*, pages 2309–2319, 2021. 7, 8
- [39] Yajun Qiu, Ruxin Wang, Dapeng Tao, and Jun Cheng. Embedded block residual network: A recursive restoration model for single-image super-resolution. In *Proceedings of the IEEE/CVF international conference on computer vision*, pages 4180–4189, 2019. 6
- [40] Jaesung Rim, Haeyun Lee, Jucheol Won, and Sunghyun Cho. Real-world blur dataset for learning and benchmarking deblurring algorithms. In *European Conference on Computer Vision*, pages 184–201. Springer, 2020. 7, 8
- [41] A. S. Saqlain, L. Y. Wang, and F. Fang. Sl-cycleGAN: Blind motion deblurring in cycles using sparse learning. 2021. 2
- [42] Christian J Schuler, Michael Hirsch, Stefan Harmeling, and Bernhard Schölkopf. Learning to deblur. *IEEE transactions on pattern analysis and machine intelligence*, 38(7):1439–1451, 2015. 1, 3
- [43] Wen-Ze Shao, Yuan-Yuan Liu, Lu-Yue Ye, Li-Qian Wang, Qi Ge, Bing-Kun Bao, and Hai-Bo Li. Deblurgan+: Revisiting blind motion deblurring using conditional adversarial networks. *Signal Processing*, 168:107338, 2020. 3
- [44] Ziyi Shen, Wenguan Wang, Xiankai Lu, Jianbing Shen, Haibin Ling, Tingfa Xu, and Ling Shao. Human-aware motion deblurring. In *Proceedings of the IEEE/CVF International Conference on Computer Vision*, pages 5572–5581, 2019. 7
- [45] W. Shi, J. Caballero, F Huszár, J. Totz, and Z. Wang. Real-time single image and video super-resolution using an efficient sub-pixel convolutional neural network. *IEEE*, 2016. 4
- [46] Karen Simonyan and Andrew Zisserman. Very deep convolutional networks for large-scale image recognition. *arXiv preprint arXiv:1409.1556*, 2014. 7
- [47] Maitreya Suin, Kuldeep Purohit, and AN Rajagopalan. Spatially-attentive patch-hierarchical network for adaptive motion deblurring. In *Proceedings of the IEEE/CVF Conference on Computer Vision and Pattern Recognition*, pages 3606–3615, 2020. 7, 8
- [48] Jian Sun, Wenfei Cao, Zongben Xu, and Jean Ponce. Learning a convolutional neural network for non-uniform motion blur removal. In *Proceedings of the IEEE conference on computer vision and pattern recognition*, pages 769–777, 2015. 1
- [49] X. Tao, H. Gao, Y. Wang, X. Shen, J. Wang, and J. Jia. Scale-recurrent network for deep image deblurring. *IEEE*, 2018. 1, 2, 3, 7, 8, 9
- [50] P. Tran, A. Tran, Q. Phung, and M. Hoai. Explore image deblurring via blur kernel space. 2021. 2
- [51] L. Wang, Y. Wang, X. Dong, Q. Xu, and Y. Guo. Unsupervised degradation representation learning for blind super-resolution (cvpr’2021). 2021. 3
- [52] Haiyan Wu, Yanyun Qu, Shaohui Lin, Jian Zhou, Ruizhi Qiao, Zhizhong Zhang, Yuan Xie, and Lizhuang Ma. Contrastive learning for compact single image dehazing. In *Proceedings of the IEEE/CVF Conference on Computer Vision and Pattern Recognition*, pages 10551–10560, 2021. 3, 5, 7
- [53] Y Yuan, W. Su, and D. Ma. Efficient dynamic scene deblurring using spatially variant deconvolution network with optical flow guided training. In *2020 IEEE/CVF Conference on Computer Vision and Pattern Recognition (CVPR)*, 2020. 7, 8
- [54] Syed Waqas Zamir, Aditya Arora, Salman Khan, Munawar Hayat, Fahad Shahbaz Khan, Ming-Hsuan Yang, and Ling Shao. Multi-stage progressive image restoration. In *Proceedings of the IEEE/CVF Conference on Computer Vision and Pattern Recognition*, pages 14821–14831, 2021. 7, 8, 9
- [55] Hongyi Zhang, Moustapha Cisse, Yann N Dauphin, and David Lopez-Paz. mixup: Beyond empirical risk minimization. *arXiv preprint arXiv:1710.09412*, 2017. 5
- [56] H. Zhang, Y. Dai, H. Li, and P. Koniusz. Deep stacked hierarchical multi-patch network for image deblurring. *IEEE*, 2019. 1, 7, 8, 9
- [57] Jiawei Zhang, Jinshan Pan, Jimmy Ren, Yibing Song, and Ming Hsuan Yang. Dynamic scene deblurring using spatially variant recurrent neural networks. In *2018 IEEE/CVF Conference on Computer Vision and Pattern Recognition (CVPR)*, 2018. 1, 2, 3, 5, 7, 8, 9
- [58] Kaihao Zhang, Wenhan Luo, Yiran Zhong, Lin Ma, Bjorn Stenger, Wei Liu, and Hongdong Li. Deblurring by realistic blurring. In *Proceedings of the IEEE/CVF Conference on Computer Vision and Pattern Recognition*, pages 2737–2746, 2020. 7, 8
- [59] Richard Zhang, Phillip Isola, and Alexei A Efron. Colorful image colorization. In *European conference on computer vision*, pages 649–666. Springer, 2016. 3
- [60] Yulun Zhang, Kunpeng Li, Kai Li, Lichen Wang, Bineng Zhong, and Yun Fu. Image super-resolution using very deep residual channel attention networks. In *Proceedings of the European conference on computer vision (ECCV)*, pages 286–301, 2018. 4
- [61] Shangchen Zhou, Jiawei Zhang, Jinshan Pan, Haozhe Xie, Wangmeng Zuo, and Jimmy Ren. Spatio-temporal filter adaptive network for video deblurring. In *Proceedings of the IEEE/CVF International Conference on Computer Vision*, pages 2482–2491, 2019. 2
- [62] W. Zou, M. Jiang, Y. Zhang, L. Chen, Z. Lu, and Y. Wu. Sdwnet: A straight dilated network with wavelet transformation for image deblurring. 2021. 1, 3, 6, 7, 8